

## Effects of Curing Program on Mechanical Behavior and Water Absorption of DGEBA/TETA Epoxy Network

D. Nguyen Dang, S. Cohendoz, S. Mallarino, X. Feugas, S. Touzain

Laboratoire des Sciences de l'Ingénieur pour l'Environnement, FRE CNRS 3474, Université de la Rochelle, la Rochelle, France

Correspondence to: S. Touzain (E-mail: sebastien.touzain@univ-lr.fr)

**ABSTRACT:** Water uptake in organic coatings remains an interesting challenge for fundamental and applied researches because chemical, physical, and mechanical properties are concerned. The polymer network, which is affected by the curing program, is a key factor for water absorption. In this work, an epoxy network based on diglycidyl ether of bisphenol A and a hardener triethyltetramine was cured at different temperatures: below  $T_g$  (protocol 1) and above  $T_g$  (protocol 2). DMA, Differential Scanning Calorimetry (DSC), and FT-IR measurements showed that both protocols allow to obtain totally cured networks. However, DSC and DMA results revealed that both cured networks present different levels of homogeneity, depending on the different curing conditions, which affect the free volume and the activation volume associated with visco-elastic properties. The mechanical properties of free films and water sorption behaviors were investigated as function of cured conditions. It was found that protocol 1-cured networks present higher mechanical properties and was less affected by water ingress than protocol 2-cured systems, leading to better barrier properties. These results highlight the influence of the curing program onto the heterogeneous distribution of the epoxy network. © 2013 Wiley Periodicals, Inc. *J. Appl. Polym. Sci.* 129: 2451–2463, 2013

**KEYWORDS:** coatings; ageing; properties and characterization; mechanical properties

Received 13 July 2012; accepted 15 November 2012; published online 30 January 2013

**DOI:** 10.1002/app.38843

### INTRODUCTION

Organic coatings are abundantly used to prevent metals from corrosion. Among them, epoxy-based paints are often industrially chosen, due to their low cost and their efficiency in corrosive medium like seawater.<sup>1,2</sup> The degradation of these coatings is usually due to the action of environmental factors such as water, UV, and temperature. Many studies related the influence of each ageing factor or a combination of them<sup>3–9</sup> in order to better understand the mechanisms and the best way to evaluate the coating lifetime.

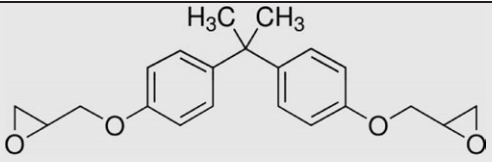
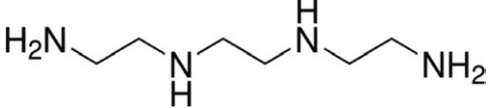
Application of an external mechanical stress is another ageing factor that has been little considered in literature. However, the mechanical state of the polymer can affect water diffusion and/or can be affected by such a process. Indeed, in previous articles,<sup>10,11</sup> we studied the effect of water uptake on two commercial paints. It was found that plasticization and hardening/softening processes can simultaneously occur within the polymer depending on the cross-linking density. It was observed that the ageing of epoxy coatings in saline solution affects the mechanical properties and then may have a significant influence on the durability. More recently,<sup>12,13</sup> it was shown that a visco-elastic mechanical stress had a strong influence onto the barrier

properties of such coatings. However, the complex formulations of these commercial systems lead to annex processes such as lixiviation that hide the real response of the polymer.

The water uptake process is mainly governed by the ambient temperature and the polymer network in terms of polarity and free volume.<sup>14–19</sup> The epoxy network is affected by the curing temperature<sup>20</sup> as well as its thermal history after a cure above the glass transition  $T_g$ . Indeed, the cooling to ambient temperature can be fast, leading to quenched material. With slower cooling rates and/or increasing the sub- $T_g$  annealing time, a physical ageing occurs leading to a density increase and mechanical properties changes.<sup>21–27</sup> This phenomenon was extensively studied in literature but the effect of a curing temperature near but below  $T_g$ , which may be encountered in some organic coatings industrial plants, has received little attention.

In order to avoid the influence of pigments, adjuvants and other fillers, a model epoxy system DGEBA/TETA was chosen to obtain the response of the sole polymer. In this article, two model epoxy networks are considered, depending on the curing program. It is expected that both networks will present different properties, allowing to precise the effect of crosslinking onto the water uptake and its effect on mechanical properties.

**Table I.** Structure and Characteristics of the Products

Product	Formula	Supplier	M (g.mol <sup>-1</sup> )	F
DGEBA		Sigma, D.E.R <sup>TM</sup> 322	340.41	2
TETA		Aldrich, DEH 24	146.23	6

## EXPERIMENTAL

### Materials

The epoxy resin used was a Diglycidyl Ether of Bisphenol A (DGEBA). As curing agent, triethylenetetramine 60% (TETA) was used. The formulae, supplier, molecular weight (M), and functionality (F) of the products are listed in Table I. All materials have been used as received without further purification.

### Sample Preparation

Stoichiometric mixture of epoxy and amine hardener was mixed at room temperature until reaching a homogeneous liquid. After degassing, the mixture was cast between two Teflon sheets which have been beforehand degreased and cleaned with acetone. The plates were separated by a spacer in order to obtain film thickness of  $120 \pm 20 \mu\text{m}$ . This system was then placed into an oven where different curing schedules were applied.

### Curing Conditions

To study effects of curing program on mechanical properties and water absorption behavior of DGEBA/TETA epoxy systems, stoichiometric mixtures of monomers were cured according to two different thermal cycles. These cycles and conversion evolution during protocol are presented in Figure 1. The rate of heating and cooling was  $2^\circ\text{C min}^{-1}$ . Both systems were heated for different times and temperatures and both protocols are identical until 31 hours (plateau at  $120^\circ\text{C}$ ). Then, protocol 1-cured samples are cooled down while protocol 2-cured samples are submitted to an additional temperature plateau at  $150^\circ\text{C}$  for 1 h. It is worth noting that final temperature of protocol-1 is lower than the glass transition temperature of our epoxy systems (as seen below) whereas it is higher in the case of protocol-2, as discussed later.

The cured specimens were stored in a desiccator containing silica gel desiccant to prevent moisture absorption before immersion.

### FTIR and DSC Measurements

Fourier transform infrared (FTIR) measurements on cured materials were performed with the Thermo-Nicolet Nexus spectrometer equipped with a Smart MIRacle ATR accessory with a diamond crystal. Spectra were recorded with a resolution of

$8 \text{ cm}^{-1}$  and at least 128 scans with the wavenumber range  $600\text{--}4000 \text{ cm}^{-1}$ .

In order to determine the glass transition temperature ( $T_g$ ), the enthalpy of reaction ( $\Delta H$ ) and the degree of cure (conversion  $\alpha$ ), Differential Scanning Calorimetry (DSC) analyses were performed on a DSC Q100 TA Instruments under nitrogen purge. The DGEBA/TETA formulations (about 10 mg) were heated from  $20$  to  $200^\circ\text{C}$  with a heating rate of  $10^\circ\text{C min}^{-1}$  under a nitrogen flow of  $50 \text{ mL min}^{-1}$ . The enthalpy of reaction  $\Delta H$  was determined from this scan. The total enthalpy of reaction ( $\Delta H_T$ ) was determined by analyzing an uncured sample ( $t_{\text{cure}} = 0$ ). The partially cured samples at different temperature and time were analyzed to determine the residual enthalpy of reaction ( $\Delta H_R$ ). The conversion  $\alpha(\%)$  was calculated as follows:

$$\alpha(\%) = \frac{\Delta H_T - \Delta H_R}{\Delta H_T} * 100 \quad (1)$$

The glass transition temperature,  $T_g$ , is taken at the half height of the change in heat capacity (middle of transition).

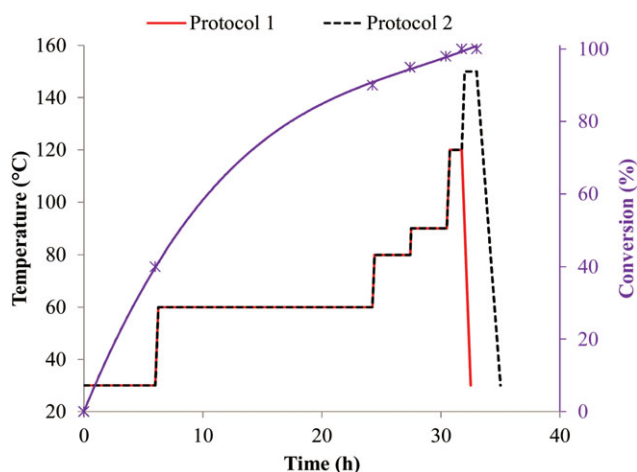


**Figure 1.** Curing conditions of DGEBA/TETA epoxy resin. [Color figure can be viewed in the online issue, which is available at [wileyonlinelibrary.com](http://wileyonlinelibrary.com).]

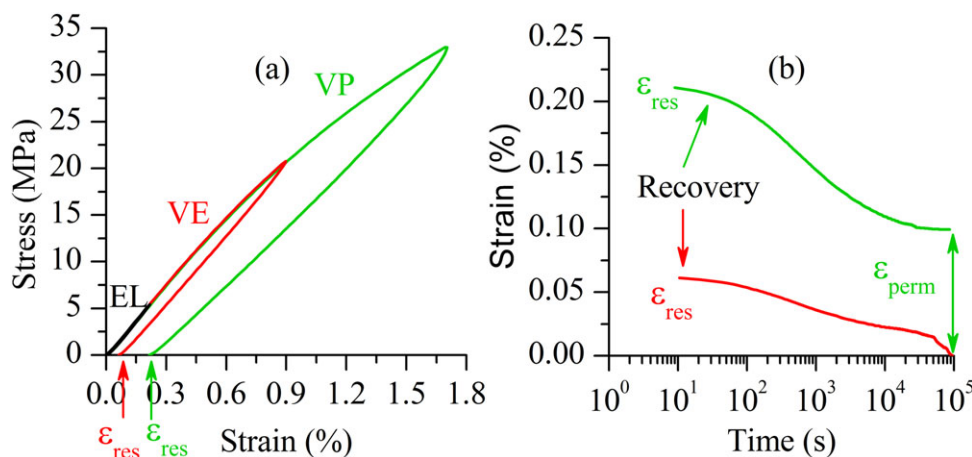


**Figure 2.** Experimental results in loading-unloading recovery tests of protocol 1-cured DGEBA/TETA network: (a) stress–strain curve, (b) recovery versus time. [Color figure can be viewed in the online issue, which is available at [wileyonlinelibrary.com](http://wileyonlinelibrary.com).]

### Mechanical Measurements

Dynamic mechanical properties of specimens were analyzed using a Dynamic Mechanical Thermal Analyzer – tensile mode (Q800 TA Instruments). Both single frequency (at 1 Hz) and multi-frequency sweeps (at 1, 2, 3, 5, 10, 20, 30, 50 Hz) were used with the heating rate  $3^{\circ}\text{C min}^{-1}$  from room temperature to  $180^{\circ}\text{C}$ . Peak maximum of  $\tan(\delta)$  curve was used as an indicator of the glass transition temperature ( $T_g$ -DMA). To investigate the time/temperature relation, WLF phenomenology is used<sup>28</sup>:

$$\log a_T = \log \left( \frac{\tau}{\tau_g} \right) = \frac{-C_1(T - T_g)}{C_2 + (T - T_g)} \quad (2)$$

Where  $a_T$  is the ratio of the relaxation time  $\tau$  at temperature  $T$  to the relaxation time  $\tau_g$  at glass transition temperature  $T_g$  and  $C_1$  and  $C_2$  are constants characteristic of the studied polymer. The  $C_1$  parameter is related to the free volume fraction  $f$  by:

$$C_1 = \frac{B}{2.303f} \quad (3)$$

where  $B$  is usually set arbitrarily equal to the unity.<sup>29</sup>

Visco-elasto plastic behavior of the DGEBA/TETA networks was characterized by DMA using a loading–unloading recovery test.<sup>30,31</sup> In this test (Figure 2), the DGEBA/TETA network is stressed up to a strain level  $\varepsilon$  corresponding to a maximal stress  $\sigma_{\text{max}}$ . Then, the stress direction is reversed and the material is placed in an unloading state [Figure 2(a)]. As soon as the stress is zero, this one is maintained at this value in order to follow the recovery of the deformation [Figure 2(b)]. When the initial strain  $\varepsilon$  is very low, the recovery is instantaneous in the unloading stage. This case characterizes the elastic (EL) domain which means that the polymer recovers instantaneously its mechanical properties after the strain (reversible process). When the applied stress increases, the measured strain is non-null after unloading (resultant strain  $\varepsilon_{\text{res}}$ ) and the polymer needs some time in order to recover totally its mechanical properties after the strain (reversible process). That is namely the visco-elastic (VE) behavior. In EL and VE domains, only the motion of polymer

chains is involved. If the strain is higher, it induces irreversible changes in the mechanical and structural properties of the polymer and the recovery is not total (permanent strain after unloading  $\varepsilon_{\text{perm}}$ ): this is the viscoplastic (VP) domain (irreversible process) where motion of polymer chains and the bond breakdown are involved.<sup>31</sup> By varying the stress–strain state in these loading–unloading recovery tests, the limits between the mechanical domains (EL/VE and VE/VP) can be estimated.

In order to study thermodynamic processes associated with visco-elasticity and visco-plasticity, another kind of test namely relaxation test was performed using DMA-tensile mode. Using classical thermal activity theory initiated by Eyring<sup>32</sup> and applied for solid polymers,<sup>30,31,33</sup> the strain rate sensitivity of the flow stress can be directly linked with molecular processes. Especially, the activation volume,  $V_a$  is associated with the jump of a molecular segment over energy barrier.<sup>10</sup> In stress relaxation test,  $V_a$  is expressed as follows:

$$V_a = k_B T \left[ \frac{d \ln(\dot{\varepsilon}_v)}{d \sigma} \right]_{\mu_s, T} \quad (4)$$

and 
$$\dot{\varepsilon}_v = \frac{\dot{\sigma}}{E} \quad (5)$$

where  $k_B$  is the Boltzmann constant, ( $\mu_s, T$ ) are a constant microstructure and temperature,  $\dot{\varepsilon}_v$  is the strain rate,  $\dot{\sigma}$  is the stress rate and  $E$  is the Young modulus.

### Water Absorption Measurements

The specimens ( $5 \times 5 \text{ cm}^2$ ) were immersed in deionized water and a NaCl 3wt% solution at 30, 40, 50, and  $60^{\circ}\text{C}$ , respectively. The samples were regularly removed from the solution, carefully wiped with a filter paper and mass measures were performed with a PRECISIA balance ( $10^{-5}\text{g}$  precision). The mass water absorbed percentage  $M_t$  (%) by the specimens was calculated with the following expression:

$$M_t(\%) = \frac{W_t - W_0}{W_0} * 100 \quad (6)$$

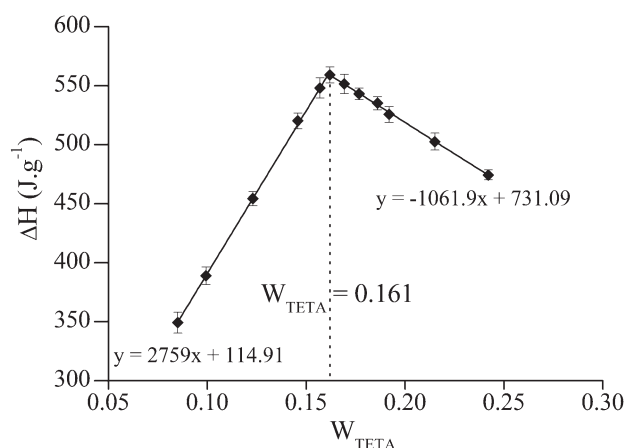


**Figure 3.** Enthalpy of reaction DGEBA/TETA as a function of mass fraction of TETA.

where  $W_t$  is the mass of the wet specimen at time  $t$ ,  $W_0$  is the mass of the dry specimen. Each point in the sorption curves represents the average of three or four experiments. The average standard deviation corresponds to a value  $<0.05\%$  on the  $M_t(\%)$  scale.

## RESULTS AND DISCUSSIONS

### Stoichiometric Proportion

The formulation based on TETA curing agent was firstly studied to investigate the stoichiometric proportion of the amine related to the epoxy resin. The enthalpy of reaction  $\Delta H$  was determined as a function of the mass fraction of TETA,  $W_{TETA}$ , by using DSC analysis. The mass fraction of TETA,  $W_{TETA}$ , was calculated with the following expression:

$$W_{TETA} = \frac{m_{TETA}}{m_{TETA} + m_{DGEBA}} \quad (7)$$

where  $m_{TETA}$  and  $m_{DGEBA}$  are the amine and epoxy masses presented in the mixture. According to the literature,<sup>34,35</sup> the extent of cure is expected to be maximal at the stoichiometric epoxy/amine ratio; therefore, the highest value of  $\Delta H$  is expected.

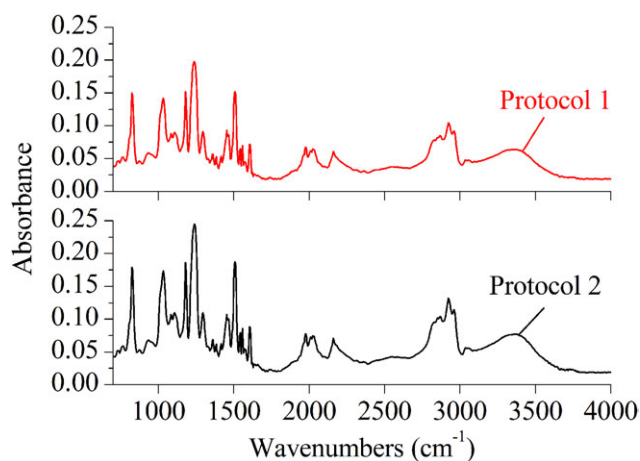


**Figure 4.** IR spectra of DGEBA/TETA cured networks. [Color figure can be viewed in the online issue, which is available at [wileyonlinelibrary.com](http://wileyonlinelibrary.com).]

Figure 3 shows the dependence of reaction with mass fraction of TETA. The TETA formulation presented an intersection of the experimental values at  $W_{TETA} = 0.161 \pm 0.005$ . The maximal  $\Delta H$  value at the intersection was found to be  $560 \pm 10$  ( $J g^{-1}$ ). This value is in agreement with other studies.<sup>34</sup>

The stoichiometric mixture of DGEBA/TETA were cured using different protocols (Figure 1). According to eq. (1), the degree of cure was calculated. The DGEBA/TETA samples were completely cured ( $\alpha = 100\%$ ) after being applied the curing protocols 1 or 2 (Figure 1). It can be noted that with a curing temperature below  $T_g$  (as seen below), protocol 1 allows the same conversion degree than protocol 2. Since no difference between both protocols was observed, it means that protocol 1 affords the epoxy-amine system enough time and energy to react totally.

### General Characterization

**FTIR.** IR spectra show that there was no difference of major bands between the samples cured by protocol 1 and protocol 2 (Figure 4). These major bands are in agreement with the results reported in literature for DGEBA/TETA resins.<sup>35,36</sup> Furthermore, we observe that there was no absorption band around  $915\text{ cm}^{-1}$  attributed by the vibration of epoxide groups.<sup>35,36</sup> IR spectra suggest that both samples are completely crosslinked and there is no difference of overall chemical properties: both protocols allow obtaining the same chemical bonds. The conversion of both protocols-cured networks will be verified by the DSC and DMA techniques in the next sections.

**Differential Scanning Calorimetry.** DSC results of totally cured specimens are presented in Figure 5. DGEBA/TETA samples cured by both protocol 1 and protocol 2 present the same  $T_g$ :  $130^\circ\text{C}$ . These results are obtained from both first and second scans of DSC. The  $T_g$  value is consistent with results reported in literature.<sup>34,37</sup> Furthermore, no residual reaction enthalpy has been observed for both protocols-cured samples. The same value of  $T_g$  from both scans and the absence of an exothermic peak prove that both samples are totally cured. However, an endothermic peak nearby the  $T_g$  has been determined in the

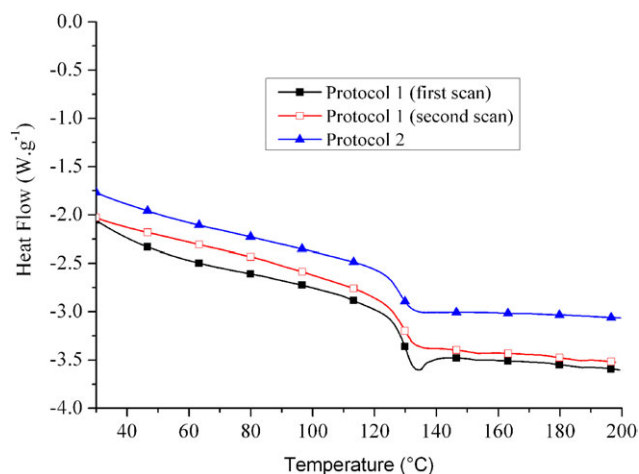


**Figure 5.** DSC scans for cured samples by protocol 1 and protocol 2. [Color figure can be viewed in the online issue, which is available at [wileyonlinelibrary.com](http://wileyonlinelibrary.com).]

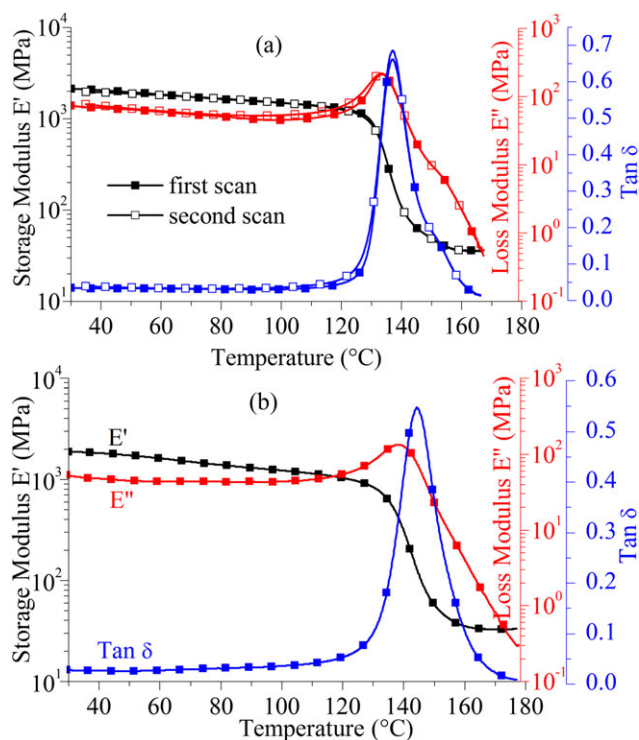


**Figure 6.** Dynamic mechanical properties of cured DGEBA/TETA network:  $\tan \delta$  as a function of temperature, measured at 1Hz. [Color figure can be viewed in the online issue, which is available at wileyonlinelibrary.com.]

first DSC scan of protocol 1-cured sample while it is not observed in the first DSC scan of protocol 2-cured sample.

The DGEBA and TETA were mixed together in a liquid state; at the beginning of the crosslinking process, the mixture was in liquid state, the amorphous crosslinked structure was permanently secured by the presence of the newly formed rigid crosslinks. Because of the rigidity and complexity of the crosslinked network, the structure existed in a glassy state or rubbery state.<sup>21</sup> It is important to note that, in protocol 1, the curing temperature is below  $T_g$ , so the DGEBA/TETA cured network was in its glassy state during curing. Long-range cooperative motions of the main chain were frozen and therefore the mobility of macromolecular segments was reduced (in comparison with that in rubbery state above  $T_g$ ). In these conditions, the amorphous network could not reconfigure itself into a purely crystalline state (ideal state). Consequently, a non-equilibrium state of material was created whose free volume ( $V$ ), enthalpy ( $H$ ), and entropy ( $S$ ) were higher than at the equilibrium state (ideal crystalline state). However, it remained sufficient mobility in the network, so more restricted molecular motions were possible at temperature close to  $T_g$ ; mobility of macromolecular segments was only reduced but not stopped.<sup>22</sup> This structural relaxation process of DGEBA/TETA macromolecules occurring in glassy state lead to a magnitude decrease of its  $V$ ,  $H$ , and  $S$ , and is referred to “physical ageing” in the literature.<sup>21–27</sup> The physical ageing occurs when the specimen is heated in the domain of ( $T_g-30^\circ\text{C}$ ) to  $T_g$  during only a few hours.<sup>26</sup> So, during protocol 1, the DGEBA/TETA network was completely cured

but a physical ageing phenomenon occurred, leading to a denser network that relaxes during the DSC scan. This phenomenon is responsible for the endothermic peak on the first DSC scan. It must be noted that a second DSC scan does not reveal this endothermic peak (Figure 5) which means that the sample has been rejuvenated during first scan. Moreover, the value of  $T_g$  is the same for both scans which supports the fact that the DGEBA/TETA network is fully cured after protocol 1.

The absence of an endothermic peak related to physical ageing in DSC curve of protocol 2-cured sample (Figure 5) can be explained by the different final curing temperatures between protocol 1 and protocol 2 (Figure 1). Indeed, the protocol 2 was built by adding a step at 150°C for 1 h to the protocol 1. This final temperature is 20°C higher than  $T_g$ . At this temperature, the DGEBA/TETA cured network was in its rubbery state and in thermodynamic equilibrium, since there was enough mobility for the molecules to achieve their most favored thermodynamic state. Thus, in order to come to its equilibrium rubbery state above  $T_g$ , the network “recovered” the  $V$ ,  $H$ ,  $S$  “lost” during the physical ageing process at glassy state.<sup>38</sup> So, the final step of heating in protocol 2 allowed to “rejuvenate” the network.<sup>21</sup> It may be understood that the network organizes itself differently from the protocol 1-cured network and more homogeneously. The cooling from 150°C to room temperature with rate 2°C min<sup>-1</sup> lead to a network change from its equilibrium rubbery state to its non-equilibrium glassy state. The time of cooling was so fast that it prevented the relaxation of network which occurs only in the domain from ( $T_g-30^\circ\text{C}$ ) to  $T_g$ . Hence, quenched systems were obtained. Finally, it can be considered that protocol 1 leads to a denser network than protocol 2-cured network.

**Dynamic Mechanical Measurement.** A typical plot of storage modulus ( $E'$ ), loss modulus ( $E''$ ), and  $\tan(\delta)$ , measured at 1Hz, as a function of temperature, is showed in Figure 6 for the protocol 1-and protocol 2-cured DGEBA/TETA networks.

Table II presents the  $T_g$  values of cured DGEBA/TETA networks determined by DMA and DSC.  $T_g$ -DMA of protocol 1-cured

**Table II.** Glass Transition Temperature of Cured DGEBA/TETA Network Determined by DSC and DMA

Curing condition	DSC		Tan $\delta$ -DMA	Ref
	$\alpha$ (%)	$T_g$ -DSC (°C)	$T_g$ -DMA (°C)	
20 h at 60°C + 24 h at 100°C	<100	-	113	[39]
Protocol 1	100	130	137	This study
24 h at RT + 2 h at 130°C	100	124	142	[34,37]
Protocol 2	100	130	144	This study
20 h at 60°C + 24 h at 100°C + XX h <sup>a</sup> at 160°C	100	-	141	[39]

RT, Room temperature;  $\alpha$ , conversion;  $T_g$ , glass transition temperature.  
<sup>a</sup>XX: not indicated in reference [39].

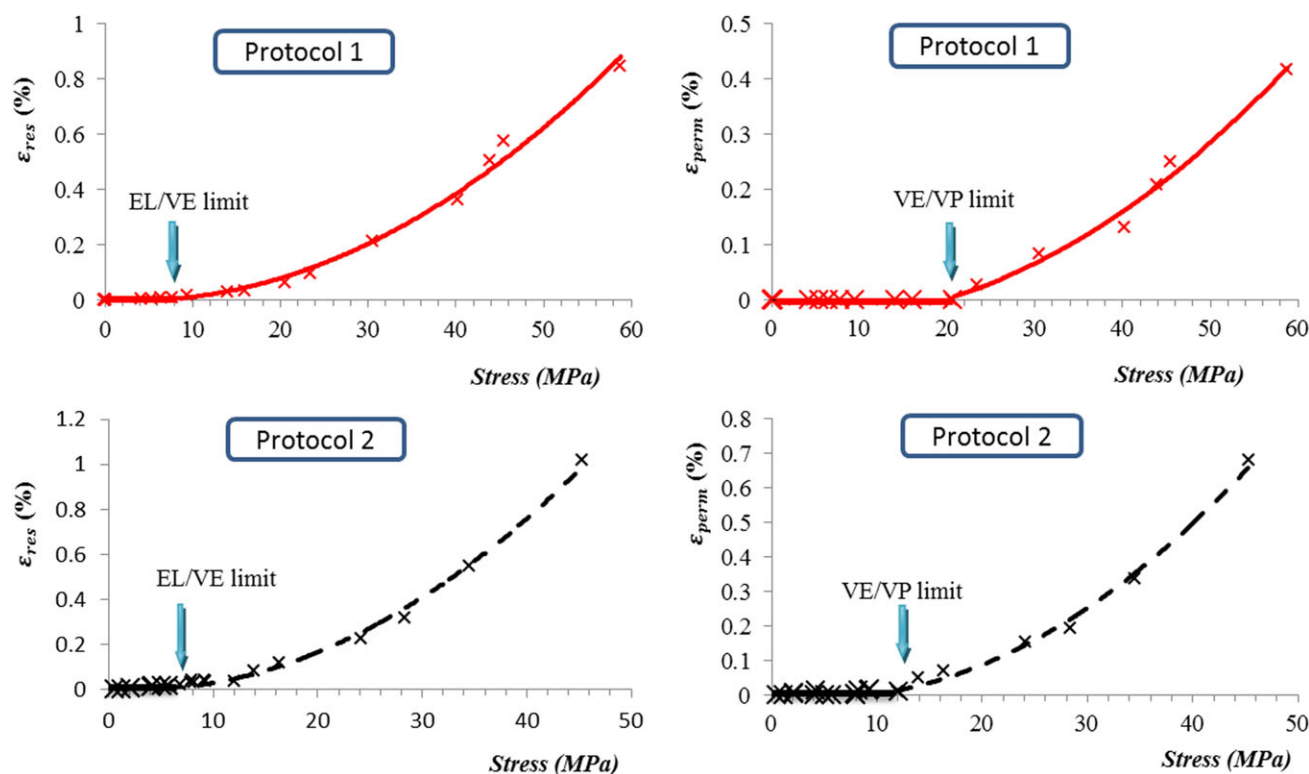
**Table III.** C1 Parameter and Free Volume Fraction ( $f$ ) of DGEBA/TETA Networks

Curing condition	C1	F (%)
Protocol 1	27	1.6
Protocol 2	24	1.8

network and protocol 2-cured network were determined to be 137°C (with a split at 153°C) and 144°C, respectively. These values are close to the results reported in literature<sup>34,37,39</sup> for fully cured systems. Besides, the  $T_g$  determined from DSC measurements is about 10°C lower than that determined by DMA, because the DSC scan provides information at the beginning of collective motion of macromolecules.<sup>40</sup>

The  $\tan(\delta)$  curve of protocol 1-cured network reveals a second small peak at 153°C which was not observed in DSC, since it is well known that DSC is less accurate than DMA. This shoulder may come from the post-reticulation of the system. In order to verify this hypothesis, a second scan with the same heating rate has been realized after finishing the first scan. Both scans are identical which means that the protocol 1 allows a complete cure of the DGEBA/TETA system. The shoulder at 153°C is always observed proving that its origin can not be due to a post-reticulation process. This shoulder was also observed on DMA spectra for DGEBA/TETA network cured with similar conditions to protocol 1 in other studies<sup>34,37</sup> where no information was given. It can be noted that the splitting of  $\tan(\delta)$  peak was noted<sup>41–44</sup> for epoxy resins after water absorption. Since at

this point no water had been in contact with the films, the presence of this shoulder can be explained by the curing conditions. Indeed, this shoulder indicates that the macromolecular structure is heterogeneous and the crosslinked network is non-uniform.<sup>27,45,46</sup> It may appear some areas with high crosslinking density (hard zone) and other ones with lower crosslinking density (soft zone) and/or a non-uniform distribution of the low-energy bonds. Both cases lead to two populations which cause the splitting of  $\tan(\delta)$  peak. For protocol 2, the DGEBA/TETA sample was heated above of  $T_g$  so there was enough mobility for the molecules to achieve their most favored thermodynamic state before cooling and the macromolecular structure could be rearranged, leading to a more homogeneous network. These findings are in agreement with the William–Landel–Ferry (WLF) approach. C1 parameters can be calculated [eq. (2)] and free volume fraction ( $f$ ) can be estimated [eq. (3)]. Free volume fraction of protocol 1-cured network is lightly lower than that of protocol 2-cured network (Table III). The free volume fraction is the ratio of free volume to total volume. It represents a volume non-occupied by the polymer molecules (an occupied volume includes not only the volume of the molecules as represented by their Van der Waals radii but also the volume associated with vibrational motions).<sup>47</sup> In the case of protocol 1, where structural relaxation occurred, the network density is higher which may lead to a greater number of weak bonds and then, to a lower free volume fraction.<sup>21</sup> It may be supposed that a protocol 2-cured sample that would have been physically aged for the same time and the same temperature used in the final step of protocol 1, would lead to the following results: a

**Figure 7.** Elasto-Visco Plastic behavior of DGEBA/TETA networks. [Color figure can be viewed in the online issue, which is available at [wileyonlinelibrary.com](http://wileyonlinelibrary.com).]

**Table IV.** Variation of the Mechanical Properties of the DGEBA-TETA Networks with the Curing Conditions

	Protocol 1	Protocol 2
$\sigma_{VE}^{EL}$ (MPa)	$8 \pm 0.5$	$6 \pm 0.5$
$\sigma_{VP}^{VE}$ (MPa)	$21 \pm 2$	$12 \pm 1$
$\epsilon_{VE}^{EL}$ (%)	$0.31 \pm 0.05$	$0.32 \pm 0.05$
$\epsilon_{VP}^{VE}$ (%)	$0.90 \pm 0.15$	$0.70 \pm 0.11$
E (MPa)	$2460 \pm 50$	$1840 \pm 60$

decrease of the storage modulus  $E'$  at the second DMA scan due to the physical ageing erasure and no shoulder in  $\tan(\delta)$  curve for both scans. Indeed, the physical ageing will not modify the free volume distribution but will only lead to a denser network.

As a conclusion, the general characterization of both cured networks indicates that there is no difference on overall chemical properties, nature of bonds. However, the free volume fraction of protocol 2-cured network is slightly higher than that of protocol 1-one but the structure of protocol 1-cured network is likely more heterogeneous due to the distribution of the free volumes or of the local densities.

### Mechanical Properties

In this section, mechanical properties including visco-elasto-plastic behavior, Young's modulus ( $E$ ), activation volume ( $V_a$ ), of both protocol 1- and protocol 2-cured DGEBA-TETA networks are examined.

Firstly, loading–unloading recovery tests (detailed in section “Mechanical Measurements”) were carried out with the variation of the stress–strain state for both protocol 1- and protocol 2-cured DGEBA-TETA networks. Thanks to these tests, curves of  $\epsilon_{res}$  and  $\epsilon_{perm}$  as function of stress can be plotted and used to determine EL/VE and VE/VP limits (Figure 7). Detailed results are presented in Table IV.

Percent elongations at the EL/VE limit and at the VE/VP limit of protocol 1-cured network are similar to that of protocol 2-cured network. However, to obtain these deformations, the applied stresses ( $\sigma_{EL/VE}$  and  $\sigma_{VE/VP}$ ) for protocol 1-cured network are higher than those for protocol 2-cured network.

The difference of mechanical properties between protocol 1- and protocol 2-cured networks can originate from the different conditions of cure leading to different non-equilibrium behaviors. According to Pascault *et al.*,<sup>48</sup> some physical properties of polymer glasses depend on their non-equilibrium character. As discussed in previous section (Dynamic Mechanical Measurement), since the physical ageing phenomenon occurred during protocol 1 in the network, the specific density of network increases so volume decreases.<sup>25</sup> Molecules in the network — from a thermodynamic point of view — change from a higher non-equilibrium position to a lower non-equilibrium position.<sup>22</sup> So, a lot of “weak bonds” can be created in the network such as Van der Waals and hydrogen bonds. Consequently, to get the similar strain, the force ( $F$ ) applied at the same sectional area ( $S$ ) in protocol 1-cured network is higher than that in protocol 2-network. In other words,

to obtain the similar values of  $\epsilon_{EL/VE}$  and  $\epsilon_{VE/VP}$ , the stresses  $\sigma_{EL/VE}$  and  $\sigma_{VE/VP}$  applied in protocol 1-cured network are higher than those applied in the other one. It is important to note that the elastic deformation corresponds to distortions of bond angles and increases of inter-atomic distances; the viscoelastic deformation corresponds to stretching of bonds between the atoms and relative chain orientation while the visco-plastic deformation leads to the motion of polymer chains and bond breakdown.<sup>31,49</sup> For both two protocols-cured networks, the types of liaisons are similar, only the number of “weak bonds” and the network structures are different. This is the reason why the  $\epsilon_{EL/VE}$  and  $\epsilon_{VE/VP}$  for both two protocols-cured networks are similar.

Secondly, Young's modulus was determined by using the slope in the early (low strain) portion of stress–strain curve (Figure 8). Protocol 1-cured network Young's modulus is higher than protocol 2-cured network one. The polymer network from protocol 1 is considered as non-homogeneous and can then be seen, in a first approach, as a “composite structure” with high chain density areas (hard zones) mixed with low chain density areas (soft zones).<sup>27,45,46</sup> The deformation of a composite involves the development of internal stress which partly explains why protocol 1 network presents a Young's modulus higher than that of protocol 2 network which has a homogeneous distribution of chain (low internal stress). Another approach is to consider the DGEBA/TETA network as a porous material. The protocol 2-cured network can be seen as a system with a homogeneous distribution of free volumes which are probably percolated at a microstructural scale. In contrast, for protocol 1-cured network, it can be considered that the local free volumes are heterogeneously distributed which leads to the formation of a non-percolated structure.<sup>50</sup> For an equivalent pore density, the material with a percolated structure is less rigid than the non-percolated one. So, both analyses (internal stress, percolation of free volumes) allow to explain the experimental results.

Figure 9 shows  $\ln(\dot{\epsilon}_v)$ - $\sigma$  curves for both protocols-cured networks when a 0.1% strain was applied. The activation volume

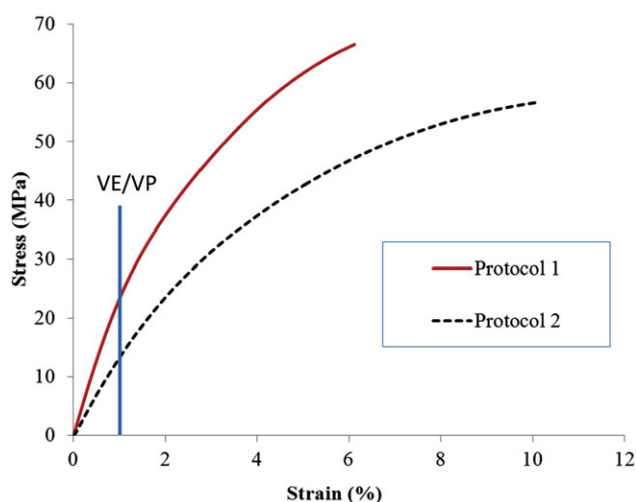


**Figure 8.** Stress–strain curves of two protocol 1- and protocol 2-cured DGEBA/TETA networks. [Color figure can be viewed in the online issue, which is available at [wileyonlinelibrary.com](http://wileyonlinelibrary.com).]

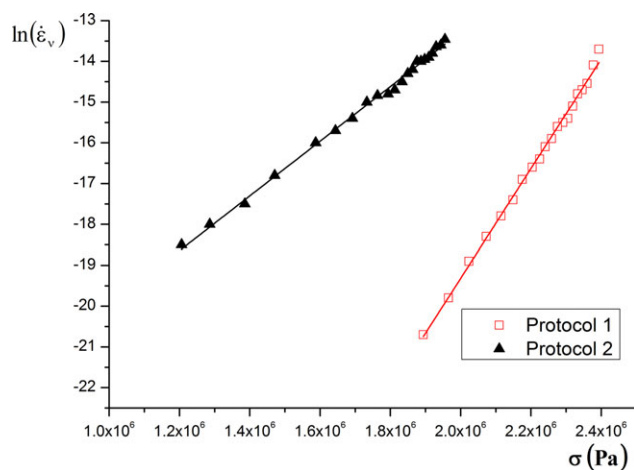


**Figure 9.**  $\ln(\dot{\epsilon}_v)$ - $\sigma$  curves when strain 0.001 applied for both protocols-cured DGEBA/TETA networks (VE range). [Color figure can be viewed in the online issue, which is available at [wileyonlinelibrary.com](http://wileyonlinelibrary.com).]

$V_a$  was determined by using the slope of this curve. The evolution of  $V_a$  is presented in Figure 10.

For both cured networks, more important  $V_a$  value is obtained for smaller strain. Then, activation volume value decreases with strain. Finally, the activation volume values stabilize when the networks are in the VP domain ( $\epsilon > \epsilon_{VE/VP}$ ). In this domain, the values of activation volume are similar for both protocols-cured networks whereas in the elastic and visco-elastic domains,  $V_a$  of protocol 1-cured network is higher than that of protocol 2-cured network.

$V_a$  is associated with the volume of polymer segment that must move to cause flow or plastic deformation and can be described as the product of a displacement vector and the area swept out by a plastic event, at the top of energy barrier.<sup>10,51–53</sup> In the case of low strain ( $\epsilon < \epsilon_{VE/VP}$ ), large  $V_a$  values are obtained because the polymer chains are in their most favorable thermodynamic state, with a lot of freedom degrees. In the case of high strain ( $\epsilon > \epsilon_{VE/VP}$ ), the polymer chains are perturbed, elongated, and they have less freedom degrees, most of the “weak bonds” existing in both networks being modified or destroyed. The  $V_a$  of both two protocols-cured networks is then similar in the plastic domain.

The larger  $V_a$  values for protocol 1-cured network, obtained for lower stresses, can be explained as follows. First, since this network was found to be heterogeneous with soft and hard zones, it may be considered that an average response is obtained, mainly governed by soft zones where weak bonds are not numerous. In other words, the viscoelasticity of protocol 1-cured network is associated with the “soft zone” (lower density of chains) where the local free volume available for the mobility of chains is important and higher than that of protocol 2-cured network where the free volume is more homogeneously distributed. Secondly, the physical ageing may also be considered. Indeed, with a denser network, the crosslinking nodes get closer with spatial rearrangements of the polymer chains that are less elongated. Therefore, when mechanically solicited, these

polymer chains may present longer displacements before a plastic deformation occurs, which means a larger activation volume.

### Hygrothermal Ageing

**Water Uptake.** Sorption experiments in deionized water and NaCl 3wt% solution of both two cured networks at 30, 40, 50, 60°C are showed in Figure 11. The detailed results are presented in Table V.

From Figure 11 and Table V, it is obvious that the equilibrium water uptake  $M_s$  slightly increases with increasing temperature because of thermal expansion.<sup>54</sup> At the same temperature,  $M_s$  in protocol 2-cured network is higher than  $M_s$  in protocol 1-cured network:  $M_s$  values are around 4% and 5% respectively for protocol 1- and protocol 2-network, although the free volume is below 2% in both networks. We previously observed (section “Mechanical properties”) that the free volume in protocol 1-network was slightly lower than that in protocol 2-network. It may partially explain why  $M_s$  in protocol 1-network is lower than that in protocol 2-network. However, since both networks are chemically identical with the same polarity and bonds nature, the main reason may come from the more homogeneous structure of protocol 2-cured networks where free volumes are percolated. Hence, the water can easily go through the network, occupying more free space within the polymer network. This is consistent with earlier studies<sup>27</sup> that showed that the equilibrium water sorption level decreases with physical ageing that was observed for protocol 1-cured polymers. The fact that the water uptake (4–5%) is higher than the free volume (2%) can be explained by water molecule interactions. Indeed, the water not only penetrates in the void spaces of the network but also forms hydrogen bonds with polar groups, causing swelling in the water-penetrated resin networks.<sup>54,55</sup>

It is important to note that  $M_s$  depends not only on the macrostructure of polymer but also on the environment.  $M_s$  is lower in the case NaCl 3wt% solution in comparison with deionized water for all temperatures tests and for both cured networks. When water contains solutes, its vapor pressure decreases

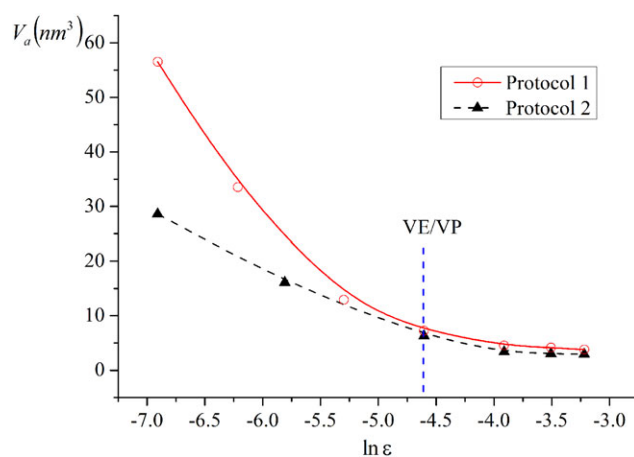


**Figure 10.** Evaluation of activation volume as a function of  $\ln(\epsilon)$ . [Color figure can be viewed in the online issue, which is available at [wileyonlinelibrary.com](http://wileyonlinelibrary.com).]



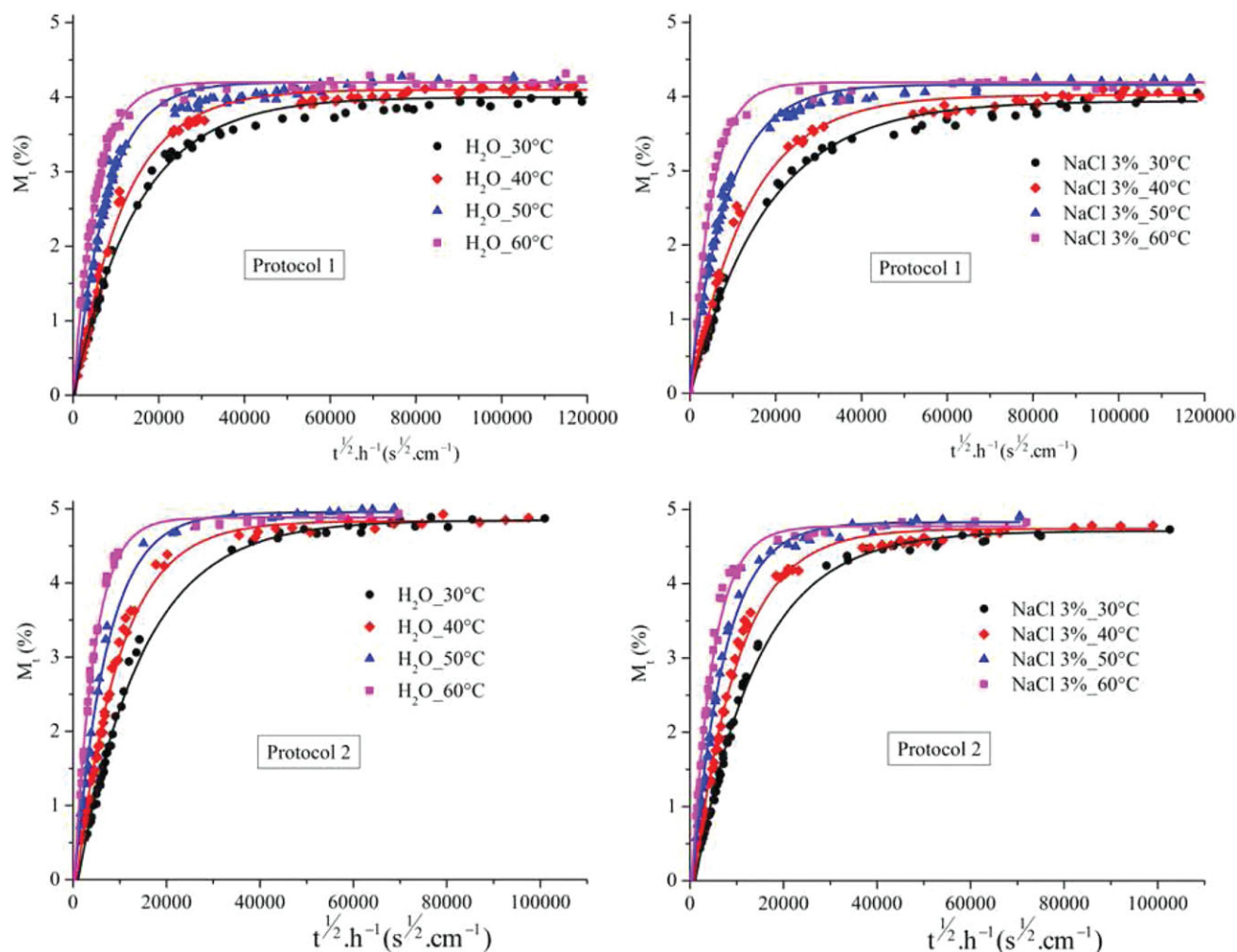


**Figure 11.** Water absorption curves of cured networks immersed in H<sub>2</sub>O and NaCl 3wt% at different temperatures. [Color figure can be viewed in the online issue, which is available at [wileyonlinelibrary.com](http://wileyonlinelibrary.com).]

(reduction of chemical potential of the liquid solvent as a result of the presence of solute).<sup>56</sup> Therefore, the equilibrium water sorption is a decreasing function of the solute concentration: saline solution is less active than pure water.<sup>48,57</sup>

The water equilibrium concentration  $C_{\infty}$  can be calculated<sup>48</sup>:

$$C_{\infty} = \frac{\rho_w}{0.018} \left( \frac{M_S}{1 + M_S} \right) \quad (\text{mol m}^{-3} \text{ if } \rho_w \text{ is expressed in kg m}^{-3}) \quad (8)$$

where  $\rho_w$  is the polymer's density in the wet state.

$C_{\infty}$  is linked to the water vapor pressure  $p$ . For a low-to-moderate hydrophilic behavior, Henry's law is valid:

$$C_{\infty} = S * p \quad (9)$$

where  $S$  is the solubility coefficient,  $p$  is the saturated vapor pressure (Pa).

In the domain of validity of Henry's law, the equilibrium concentration is proportional to the relative hygrometry. Immersion in pure water must lead to the same result as in a saturated atmosphere.<sup>48</sup>

**Table V.** Equilibrium Water Uptake  $M_s(\%)$  of Cured Networks Immersed in H<sub>2</sub>O and NaCl 3wt% at Different Temperatures

Temperature (°C)	$M_s(\%)_{H_2O}$		$M_s(\%)_{NaCl \ 3wt\%}$	
	Protocol 1	Protocol 2	Protocol 1	Protocol 2
30	4.00 ± 0.05	4.80 ± 0.04	3.94 ± 0.02	4.70 ± 0.03
40	4.08 ± 0.02	4.82 ± 0.01	3.99 ± 0.03	4.78 ± 0.02
50	4.20 ± 0.01	4.98 ± 0.01	4.15 ± 0.02	4.91 ± 0.01
60	4.22 ± 0.01	4.93 ± 0.01	4.18 ± 0.05	4.83 ± 0.04

From eqs. (8), (9), the solubility  $S$  is given by:

$$S = \frac{c_\infty}{p} = \frac{\rho_w}{0.018p} \left( \frac{M_S}{1 + M_S} \right) \quad (\text{mol} \cdot \text{m}^{-3} \cdot \text{Pa}^{-1}) \quad (10)$$

The saturated vapor pressure,  $p$ , increases with temperature. In a first approximation, it can be written:

$$p = p_0 \exp\left(-\frac{H_w}{RT}\right) \quad (11)$$

where  $\ln(p_0) = 25.33$  ( $p_0$  in Pa) and the heat of vaporization of water is:  $H_w = 42.8 \text{ kJ mol}^{-1}$ . It can be noted that if water contains solutes NaCl 3wt%, its vapor pressure,  $p_{\text{VNaCl}}^{\text{H}_2\text{O}}$ , decreases according to Raoult's law (when NaCl is placed in water, the salt dissolves into its component ions, that do not vaporize).

The solubility  $S$  obeys an Arrhenius law:

$$S = S_0 \exp\left(-\frac{H_s}{RT}\right) \quad (12)$$

where  $H_s$  is the heat of dissolution (enthalpy of solubility). In the case of water,  $H_s$  is negative (the dissolution process is

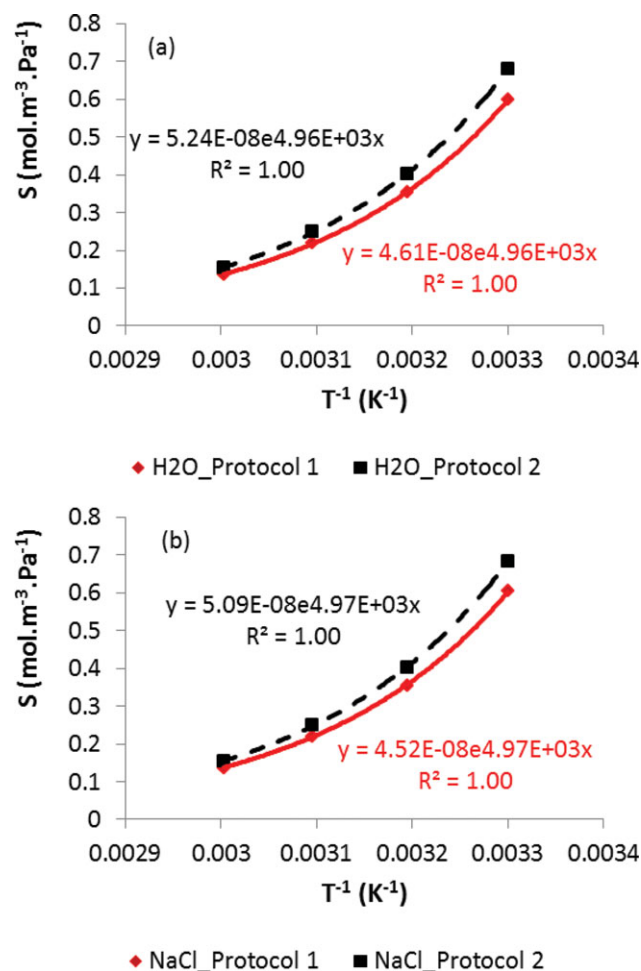


**Figure 12.** Solubility- $T^{-1}$  curves of the cured networks immersed in (a)  $\text{H}_2\text{O}$  and (b) NaCl 3wt%. [Color figure can be viewed in the online issue, which is available at [wileyonlinelibrary.com](http://wileyonlinelibrary.com).]

**Table VI.** Arrhenius Parameters Applied for the Water Dissolution Process

Solution	$S_0$ ( $\text{mol m}^{-3} \text{ Pa}^{-1}$ )	
	Protocol 1	Protocol 2
$\text{H}_2\text{O}$	$4.6 \times 10^{-8}$	$5.2 \times 10^{-8}$
NaCl 3%	$4.5 \times 10^{-8}$	$5.1 \times 10^{-8}$

exothermic) and ranges generally from  $-25 \text{ kJ mol}^{-1}$  (polymer of low polarity) to  $-50 \text{ kJ mol}^{-1}$  (highly polar polymers).<sup>48</sup>

It can be noted that the evolutions of these two factors,  $S$  and  $p$ , with temperature are antagonistic:  $p$  increases with temperature while  $S$  decreases. Finally,  $C_\infty$  can be written as:

$$C_\infty = S * p = S_0 p_0 \exp\left[-\frac{(H_s + H_w)}{RT}\right] \quad (13)$$

The density  $\rho$  of protocol 1- and protocol 2-networks are 1174 and 1137  $\text{kg m}^{-3}$ , respectively. By using the result of water equilibrium sorption and the above equations, the enthalpy of solubility  $H_s$  and  $S_0$  are determined (Figure 12). We can assume that identical low energy bonds are formed in both networks, so  $H_s$  is the same for both networks, an average value being  $-41.2 \text{ kJ mol}^{-1}$ . The values of  $S_0$  are then presented in Table VI.

Equation 10 shows that  $C_\infty$  (and  $M_S$ ) depends on two factors: solubility coefficient  $S$  and vapor pressure  $p$ .  $S$  depends not only on the "contain" capacity of the polymer networks ( $S_0$ ) but also on the polymer-water interactions ( $H_s$ ). According to Tcharkhtchi *et al.*,<sup>58</sup> the water dissolution in the epoxide-amine system is due to the formation of strong hydrogen bonds between the water molecules and the hydroxyl groups (polar groups) of network and highly exothermic. This is the reason why  $H_s$  is independent of networks (protocol 1 or protocol 2: completely cured) and types of solution (NaCl 3wt% or pure water). So, our results can be explained as follows:

- (1) at a given temperature, independently from the ageing solution, the hydrophilic sites of the protocol 1-cured network (heterogeneous and physical aged network) are fewer than that of protocol 2-one (less heterogeneous and no physical ageing):  $S_0^{\text{protocol1}} < S_0^{\text{protocol2}}$ . Therefore, equilibrium water sorption  $C_\infty$  (and  $M_S$ ) in protocol 1-network is lower than that in protocol 2-one;
- (2) at a given temperature, independently from the curing protocol,  $C_\infty$  and  $M_S$  depend both on the partial vapor pressure  $p$  and on  $S_0$ . The presence of nonvolatile substance (NaCl) in water leads to the decrease of  $p$  (Raoult's law). On the other hand, the water molecules in the NaCl 3wt% solution can form fewer hydrogen bonds with polar groups of the networks than in pure water:  $S_0^{\text{NaCl3wt\%}} < S_0^{\text{H}_2\text{O}}$ . Thus,  $C_\infty$  (and  $M_S$ ) in NaCl 3wt% is lower than that in pure water;
- (3) independently from the ageing solution and the cured-network,  $C_\infty$  and  $M_S$  increase slightly with temperature. It is interesting to remark that  $C_\infty$  (and  $M_S$ ) is governed by two antagonistic factors:  $H_s$  takes a high negative

value that leads to the decrease of  $S$  when temperature increases. On the other hand, vapor pressure  $p$  increases with temperature (eq. 12). However, the diminution of  $S$  is lower in comparison with the increase of  $p$  in a situation where  $[H_s] < [H_w]$ .

**Diffusion.** The initial linear curves in Figure 11 indicate that diffusion of all cured networks followed the Fick law. The diffusion coefficients can be calculated with the Fick diffusion equation<sup>48</sup>:

$$\frac{M_t}{M_s} = 1 - \frac{8}{\pi^2} \sum_{n=0}^{\infty} \frac{1}{(2n+1)^2} \exp\left[-\frac{(2n+1)^2 D \pi^2}{h^2} t\right] \quad (14)$$

where  $M_t$  is the amount of absorbed water at time  $t$ ,  $M_s$  is the amount of water absorbed at saturation,  $h$  is the thickness of the freestanding specimen and  $D$  is the diffusion coefficient which is considered to be constant over the exposition time.

At sufficiently short times (when  $\frac{M_t}{M_s} < 0.5$ ), the water uptake is proportional to the square root of time:

$$\frac{M_t}{M_s} = \frac{4\sqrt{D}}{h\sqrt{\pi}} \sqrt{t} \quad (15)$$

From eq. (15), the diffusion coefficients  $D$  were calculated and presented in Table VII. From these results, regardless the testing solution, at the same temperature, the diffusion coefficient of protocol 2-cured network is always higher than that of protocol 1-cured network. The decrease of diffusion coefficients of protocol 1 network in comparison with that of protocol 2 network may originate from the physical ageing phenomenon, as shown by Kong.<sup>27</sup> On the other hand, Verdu observed that the diffusion coefficient is higher for no or little hydrogen bond networks (e.g. polyester or vinyl ester) in comparison with highly hydrogen bond network (e.g. epoxy-amine).<sup>57</sup> With a denser protocol 1 network, the formation of hydrogen bond with the polar groups is easy. The number of formed hydrogen bonds increases and/or the energy of these “weak bonds” become important (since the length of the hydrogen bond decreases). The diffusion coefficient is then influenced by the rate of disruption of epoxy/hydrogen bond and the formation of polymer-water hydrogen bond.<sup>58</sup> The same conclusion is obtained if we consider that the protocol 1-cured network has a heterogeneous distribution of free volumes. With non-percolated local free volumes, the diffusion rate is slow down.

For the same cured network, the diffusion coefficient in deionized water is superior in comparison with that in NaCl 3wt%

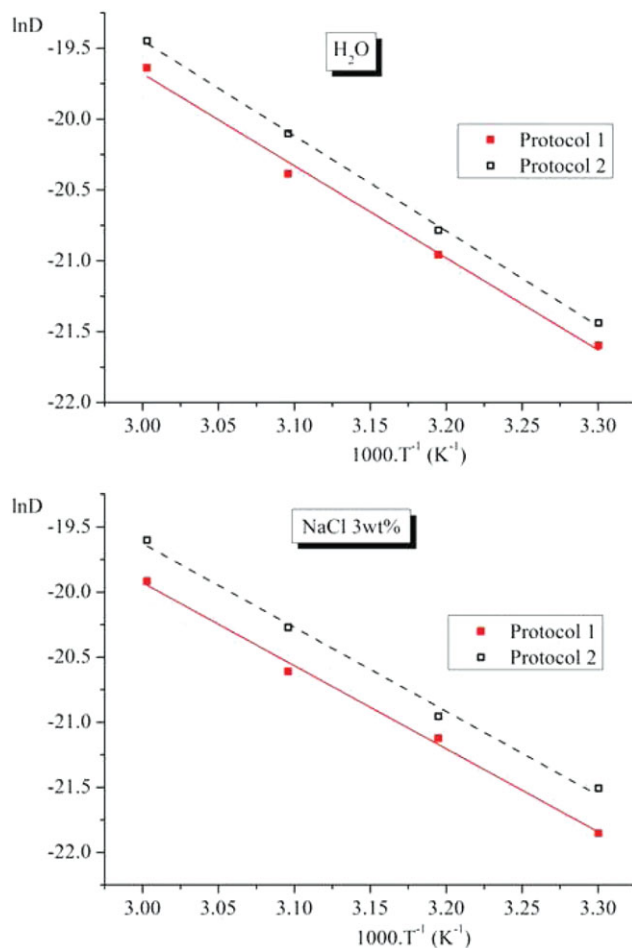


**Figure 13.** Diffusion coefficients in H<sub>2</sub>O and NaCl 3wt% at different temperatures. [Color figure can be viewed in the online issue, which is available at [wileyonlinelibrary.com](http://wileyonlinelibrary.com).]

solution. This result shows that diffusion coefficient depends not only on macromolecule of polymer network but also on the presence of solute in water. The effect of solute on the water absorption of polymer network may be explained by molecular interpretation similar to the molecular origin of Raoult’s law.<sup>48</sup> The presence of solute molecules reduces the rate at which H<sub>2</sub>O molecules leave the surface of solution to absorb into polymer network.

As seen in Table VII and Figure 13, the diffusion coefficients increase with the increase of temperature. The temperature

**Table VII.** Diffusion Coefficients  $D$  for Cured Networks Immersed in H<sub>2</sub>O and NaCl 3wt% at Different Temperatures

Temperature (°C)	$D \times 10^{10}(\text{cm}^2 \text{ s}^{-1})_{\text{H}_2\text{O}}$		$D \times 10^{10}(\text{cm}^2 \text{ s}^{-1})_{\text{NaCl 3wt\%}}$	
	Protocol 1	Protocol 2	Protocol 1	Protocol 2
30	4.17 ± 0.12	4.89 ± 0.06	3.23 ± 0.07	4.56 ± 0.04
40	7.91 ± 0.03	9.40 ± 0.27	6.70 ± 0.02	8.31 ± 0.42
50	14.0 ± 0.17	18.6 ± 0.12	11.2 ± 0.26	17.8 ± 0.72
60	29.6 ± 0.19	35.8 ± 0.65	22.4 ± 0.6	30.7 ± 0.29

**Table VIII.** Arrhenius Parameters Applied for the Diffusion Process

Solution	$E_a$ (kJ mol <sup>-1</sup> )		$D_0$ (cm <sup>2</sup> s <sup>-1</sup> )	
	Protocol 1	Protocol 2	Protocol 1	Protocol 2
H <sub>2</sub> O	54	55.8	0.83	1.98
NaCl 3wt%	53	54.5	0.45	1.01

dependence of the diffusion coefficients can be expressed by an Arrhenius rate equation:

$$D = D_0 \exp\left(-\frac{E_a}{RT}\right) \quad (16)$$

where the pre-exponential factor  $D_0$  represents the permeability index,<sup>58</sup>  $E_a$  is the activation energy of the diffusion process,  $T$  is temperature (K) and  $R$  is the gas constant.

The values of  $E_a$  and  $D_0$  were obtained from the slope and intercept at  $1/T = 0$  (at infinite temperature) of the plot of  $\ln D$  versus  $1/T$  (Figure 13). These results are presented in Table VIII and are in agreement with the literature values for fully cured epoxy resin systems.<sup>55,59,60</sup> We observe quite similar value for  $E_a$  in agreement with other studies with DGEBA/TETA network.<sup>61</sup> However,  $D_0$  values for protocol 2 network are higher than that of protocol 1 network. These differences can be easily explained by a more homogeneous distribution of free volumes for protocol 2 network.

## CONCLUSIONS

This article discussed the effects of curing conditions on the mechanical properties and water absorption behavior in DGEBA/TETA networks and the following points have been observed:

- (1) Curing conditions affect the free volume distribution and the homogeneity of network density: in the case of protocol 1, the curing temperature is below  $T_g$  and leads to the formation of a heterogeneous network with soft and hard crosslinked zones (bimodal distribution of the free volume). For protocol 2-cured networks, where the curing temperature is above  $T_g$ , a homogeneous network is allowed to form. In other words, the bimodal distribution can be converted to a unimodal distribution by a prolonged heating above  $T_g$ . Furthermore, the different conditions of cure lead to a different number of formed hydrogen bonds and/or energy of these "weak bonds".
- (2) Due to the physical ageing phenomenon occurring in protocol 1-cured network, the free volume decreases in comparison with protocol 2-network whose the physical ageing phenomenon has been erased (thermal rejuvenation). The protocol 1 leads to different mechanical properties in comparison with protocol 2: increase of Young's modulus due to internal stresses, increase of  $\sigma_{EL/VE}$  and  $\sigma_{VE/VP}$  increase of  $V_w$  in relation with a higher heterogeneity and a free volume distribution.
- (3) The effect of curing conditions on the water absorption behavior of DGEBA/TETA cured networks was revealed.

The equilibrium water sorption level, diffusion coefficient, pre-exponential factor of the protocol 1-cured network decrease in comparison with protocol 2-cured network because of the difference of free volume and heterogeneity of networks.

- (4) The presence of NaCl in water hinders the escape of H<sub>2</sub>O molecules to absorb into DGEBA-TETA networks and leads to a slight decrease of the equilibrium water sorption level, diffusion coefficient, pre-exponential factor of both protocols-cured networks. However, it seems clear that the effect of the curing program on water absorption processes is higher than the nature of the ageing solution.

These results suggest that a curing temperature near  $T_g$  but below  $T_g$  leads to a polymer network with better barrier properties.

This work was supported by the Regional Council of Poitou-Charentes as part of the PhD thesis of NGUYEN DANG Dan.

## REFERENCES

1. Funke, W. J. *Oil Colour Chem. Assoc.* **1979**, *62*, 63.
2. Wicks, Z. W.; Jones, F. N.; Pappas, S. P.; Wicks, D. A. *Organic Coatings: Science and Technology*, 2nd ed.; Wiley-Interscience: New York, **1999**.
3. Kendig, M. W.; Leidheiser, J. H. *J. Electrochem. Soc.* **1976**, *123*, 982.
4. Beaunier, L.; Epelboin, I.; Lestrade, J. C.; Takenouti, H. *Surf. Technol.* **1976**, *4*, 237.
5. Kendig, M.; Mansfeld, F.; Tsai, S. *Corros. Sci.* **1983**, *23*, 317.
6. Mischczyk, A.; Darowicki, K. *Corros. Sci.* **2001**, *43*, 1337.
7. Yang, X. F.; Li, J.; Croll, S. G.; Tallman, D. E.; Bierwagen, G. P. *Polym. Degrad. Stab.* **2003**, *80*, 51.
8. Touzain, S.; Thu, Q. L.; Bonnet, G. *Prog. Org. Coat.* **2005**, *52*, 311.
9. Deflorian, F.; Rossi, S.; Fedrizzi, L.; Zanella, C. *Prog. Org. Coat.* **2007**, *59*, 244.
10. Fredj, N.; Cohendoz, S.; Feaugas, X.; Touzain, S. *Prog. Org. Coat.* **2010**, *69*, 82.
11. Fredj, N.; Cohendoz, S.; Mallarino, S.; Feaugas, X.; Touzain, S. *Prog. Org. Coat.* **2010**, *67*, 287.
12. Fredj, N.; Cohendoz, S.; Feaugas, X.; Touzain, S. *Prog. Org. Coat.* **2011**, *72*, 260.
13. Fredj, N.; Cohendoz, S.; Feaugas, X.; Touzain, S. *Prog. Org. Coat.* **2012**, *74*, 391.
14. Kwisnek, L.; Kaushik, M.; Hoyle, C.; Nazarenko, S. *Macromolecules* **2010**, *43*, 3859.
15. Soles, C. L.; Chang, F. T.; Bolan, B. A.; Hristov, H. A.; Gidley, D. W.; Yee, A. F. *J. Polym. Sci. Part B: Polym. Phys.* **1998**, *36*, 3035.
16. Soles, C. L.; Chang, F. T.; Gidley, D. W.; Yee, A. F. *J. Polym. Sci. Part B: Polym. Phys.* **2000**, *38*, 776.
17. Soles, C.; Yee, A. *J. Polym. Sci. Part B Polym. Phys.* **2000**, *38*, 792.
18. Bohlen, J.; Wolff, J.; Kirchheim, R. *Macromolecules* **1999**, *32*, 3766.

19. Jackson, M.; Kaushik, M.; Nazarenko, S.; Ward, S.; Maskell, R. *J. Wiggins, Polymer* **2011**, *52*, 4528.
20. Pethrick, R. A.; Hollins, E. A.; McEwan, I.; Pollock, E. A.; Hayward, D. *Polym. Int.* **1996**, *39*, 275.
21. Odegard, G. M.; Bandyopadhyay, A. *J. Polym. Sci. Part B: Polym. Phys.* **2011**, *49*, 1695.
22. Perera, D. Y. *Prog. Org. Coat.* **2003**, *47*, 61.
23. Struik, L. C. E. *Physical Aging in Amorphous Polymers and Other Materials*; Elsevier: Amsterdam, **1978**.
24. Fayolle, B.; Verdu, J. *Techniques de l'ingénieur*; AM3150, Paris, **2005**, p 19.
25. Lee, A.; McKenna, G. B. *Polymer* **1988**, *29*, 1812.
26. Fraga, F.; Castro-Diaz, C.; Rodriguez-Núñez, E.; Martinez-Ageitos, J. M. *Polymer* **2003**, *44*, 5779.
27. Kong, E. In *Epoxy Resins and Composites IV: Physical Aging in Epoxy Matrices and Composites*; Dušek, K., Ed; Springer, Berlin: Heidelberg, **1986**, p 125.
28. Williams, M. L.; Landel, R. F.; Ferry, J. D. *J. Am. Chem. Soc.* **1955**, *77*, 3701.
29. Ferry, J. D. *Viscoelastic Properties of Polymers*; Wiley: New York, **1980**, p 287.
30. Brusselle-Dupend, N.; Lai, D.; Feaugas, X.; Guigon, M.; Clavel, M. *Polym. Eng. Sci.* **2001**, *41*, 66.
31. Fredj, N.; Cohendoz, S.; Feaugas, X.; Touzain, S. *Prog. Org. Coat.* **2008**, *63*, 316.
32. Eyring, H. *J. Chem. Phys.* **1936**, *4*, 283.
33. G'Sell, C.; Jonas, J. J. *J. Mater. Sci.* **1981**, *16*, 1956.
34. Garcia, F. G.; Soares, B. G.; Pita, V. J. R. R.; Sánchez, R.; Rieumont, J. *J. Appl. Polym. Sci.* **2007**, *106*, 2047.
35. Malajati, Y. Ph-D thesis, Univ. Blaise Pascal, Clermont-Ferrand, **2009**.
36. Ngono, Y.; Marechal, Y.; Mermilliod, N. *J. Phys. Chem. B* **1999**, *103*, 4979.
37. González Garcia, F.; Leyva, M. E.; Oliveira, M. G.; De Queiroz, A. A. A.; Simões, A. Z. *J. Appl. Polym. Sci.* **2010**, *117*, 2213.
38. Arturo, H. In *Handbook of Thermal Analysis and Calorimetry, Chapter 9 Thermosets*; Stephen, Z. D. C., Ed; Elsevier Science B.V., **2002**, p 295.
39. Brown, J.; Rhoney, I.; Pethrick, R. A. *Polym. Int.* **2004**, *53*, 2130.
40. Takenouti, H. In *Prévention et lutte contre la corrosion: une approche scientifique et technique: Evaluation de la protection contre la corrosion assurée par des revêtements organiques*; Normand, B.; Pébère, N.; Richard, C.; Wery, M., Eds.; Presses polytechniques et universitaires Romandes: Lausanne, **2004**, p 775.
41. Chateauminois, A.; Chabert, B.; Soulier, J. P.; Vincent, L. *Polym. Compos.* **1995**, *16*, 288.
42. De'Nève, B.; Shanahan, M. E. R. *Polymer* **1993**, *34*, 5099.
43. Ivanova, K. I.; Pethrick, R. A.; Affrossman, S. *J. Appl. Polym. Sci.* **2001**, *82*, 3477.
44. McConnell, B. K.; Pethrick, R. A. *Polym. Int.* **2008**, *57*, 689.
45. Kinsella, E. M.; Mayne, J. E. O. *Br. Polym. J.* **1969**, *1*, 173.
46. Mayne, J. E. O.; Scantlebury, J. D. *Br. Polym. J.* **1970**, *2*, 240.
47. Marzocca, A. J.; Somoza, A.; Goyanes, S. N.; Salgueiro, W.; König, P. *Polym. Int.* **2002**, *51*, 1277.
48. Pascault, J-P.; Sautereau, H.; Williams, R. J. J.; Verdu, J. *Thermosetting Polymers*; Marcel Dekker Inc.: New York, **2002**, p 283&421.
49. Ehrenstein, G. W.; Montagne, F. *Matériaux Polymères: Structure, Propriétés et Applications*; Hermès Science Publications: Paris, **2000**.
50. Meille, S.; Garboczi, E. J. *Model. Simul. Mater. Sci. Eng.* **2001**, *9*, 371.
51. White, J. J. *J. Mater. Sci.* **1981**, *16*, 3249.
52. Rumzan, I.; Williams, J. G. *Polymer* **2000**, *41*, 4291.
53. Wendlandt, M.; Tervoort, T. A.; Suter, U. W. *Polymer* **2005**, *46*, 11786.
54. Adamson, M. J. *J. Mater. Sci.* **1980**, *15*, 1736.
55. Zhou, J.; Lucas, J. P. *Polymer* **1999**, *40*, 5505.
56. Atkins, P.; De Paula, J. *Physical Chemistry*; Oxford University Press: Oxford, **2008**, p 144, 808.
57. Verdu, J. Volume AM3165, *Techniques de l'ingénieur*, Ed. T.I., Paris, **2000**, p 8.
58. Tcharkhtchi, A.; Bronnec, P. Y.; Verdu, J. *Polymer* **2000**, *41*, 5777.
59. Musto, P.; Mascia, L.; Ragosta, G.; Scarinzi, G.; Villano, P. *Polymer* **2000**, *41*, 565.
60. Diamant, Y.; Marom, G.; Broutman, L. J. *J. Appl. Polym. Sci.* **1981**, *26*, 3015.
61. Carfagna, C.; Apicella, A.; Nicolais, L. *J. Appl. Polym. Sci.* **1982**, *27*, 105.